ELSEVIER

Catalysis Today 53 (1999) 115–129

CATALYSIS TODAY

www.elsevier.com/locate/cattod

Heterogeneous photocatalysis: fundamentals and applications to the removal of various types of aqueous pollutants

Jean-Marie Herrmann *

Photocatalyse, Catalyse et Environnement, Ecole Centrale de Lyon, BP 163, 69131 Ecully-Cedex, France

Abstract

Photocatalysis is based on the double aptitude of the photocatalyst (essentially titania) to simultaneously adsorb both reactants and to absorb efficient photons. The basic fundamental principles are described as well as the influence of the main parameters governing the kinetics (mass of catalyst, wavelength, initial concentration, temperature and radiant flux). Besides the selective mild oxidation of organics performed in gas or liquid organic phase, UV-irradiated titania becomes a total oxidation catalyst once in water because of the photogeneration of $OH^{\bullet}$ radicals by neutralization of OH^- surface groups by positive photo-holes. A large variety of organics could be totally degraded and mineralized into CO_2 and harmless inorganic anions. Any attempt of improving titania's photoactivity by noble metal deposition or ion-doping was detrimental. In parallel, heavy toxic metal ions (Hg^{2+}, Ag^+, noble metals) can be removed from water by photodeposition on titania. Several water -detoxification photocatalytic devices have already been commercialized. Solar platforms are working with large-scale pilot photoreactors, in which are degraded pollutants with quantum yields comparable to those determined in the laboratory with artificial light.

1. Principle of heterogeneous photocatalysis

Heterogeneous photocatalysis is a discipline which includes a large variety of reactions: mild or total oxidations, dehydrogenation, hydrogen transfer, O_2^{18}–O_2^{16} and deuterium-alkane isotopic exchange, metal deposition, water detoxification, gaseous pollutant removal, etc. In line with the two latter points, it can be considered as one of the new 'advanced oxidation technologies' (AOT) for air and water purification treatment. Several books and reviews have been recently devoted to this problem [1–6]. A recent review has reported more than 1200 references on the subject [7]

Heterogeneous photocatalysis can be carried out in various media: gas phase, pure organic liquid phases or aqueous solutions. As for classical heterogeneous catalysis, the overall process can be decomposed into five independent steps:

1. Transfer of the reactants in the fluid phase to the surface
2. Adsorption of a least one of the reactants
3. Reaction in the adsorbed phase
4. Desorption of the product(s)
5. Removal of the products from the interface region

The photocatalytic reaction occurs in the adsorbed phase (Step No. 3). The only difference with conventional catalysis is the mode of activation of the catalyst in which the thermal activation is replaced by a photonic activation as developed in the next paragraph. The activation mode is not concerned with Steps 1, 2,

* Tel.: +33-4-7218-6493; fax: +33-4-7833-0337
E-mail address: jean-marie.herrmann@ec-lyon.fr (J.-M. Herrmann)

0920-5861/99/$ – see front matter
PII: S0920-5861(99)00107-8

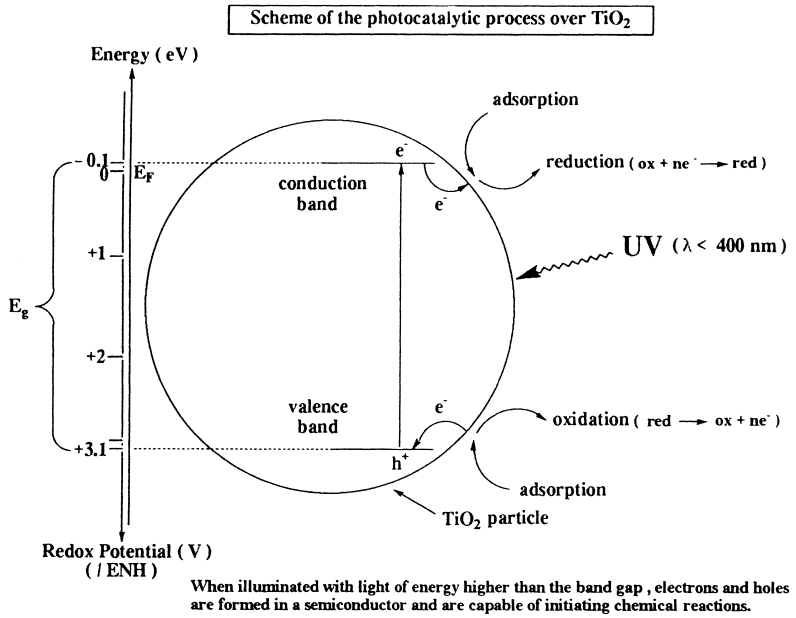

Fig. 1. Energy band diagram of a spherical titania particle.

4 and 5, although photoadsorption and photodesorption of reactants, mainly oxygen, do exist.

When a semiconductor catalyst (SC) of the chalcogenide type (oxides (TiO_2, ZnO, ZrO_2, CeO_2,...), or sulfides (CdS, ZnS,...)) is illuminated with photons whose energy is equal to or greater than their band-gap energy E_G ($h\nu \geq E_G$), there is absorption of these photons and creation within the bulk of electron-hole pairs, which dissociate into free photoelectrons in the conduction band and photoholes in the valence band. (Fig. 1)

Simultaneously, in the presence of a fluid phase (gas or liquid), a spontaneous adsorption occurs and according to the redox potential (or energy level) of each adsorbate, an electron transfer proceeds towards acceptor molecules, whereas positive photoholes are transferred to donor molecules (actually the hole transfer corresponds to the cession of an electron by the donor to the solid).

$$h\nu + (\mathrm{SC}) \rightarrow \mathrm{e}^- + \mathrm{p}^+ \quad (1)$$

$$\mathrm{A(ads)} + \mathrm{e}^- \rightarrow \mathrm{A}^- \mathrm{(ads)} \quad (2)$$

$$\mathrm{D\,(ads)} + \mathrm{p}^+ \rightarrow \mathrm{D}^+ \mathrm{(ads)} \quad (3)$$

Each ion formed, subsequently, reacts to form the intermediates and final products. As a consequence of reactions [1–3], the photonic excitation of the catalyst appears as the initial step of the activation of the whole catalytic system. Thence, the efficient photon has to be considered as a reactant and the photon flux as a special fluid phase, the 'electromagnetic phase'. The photon energy is adapted to the absorption of the catalyst, not to that of the reactants. The activation of the process goes through the excitation by the solid but not through that by the reactants: there is no photochemical process in the adsorbed phase but only a true heterogeneous photocatalytic regime as demonstrated further.

The photoefficiency can be reduced by the electron-hole recombination, described in Fig. 2, which corresponds to the degradation of the photoelectric energy into heat.

$$\mathrm{e}^- + \mathrm{p}^+ \rightarrow N + E \quad (4)$$

where N is the neutral center and E the energy released under the form of light ($h\nu' \leq h\nu$) or of heat.

2. Catalysts and photoreactors

Various chalcogenides (oxides and sulfides) have been used: TiO_2, ZnO, CeO_2, CdS, ZnS, etc. As

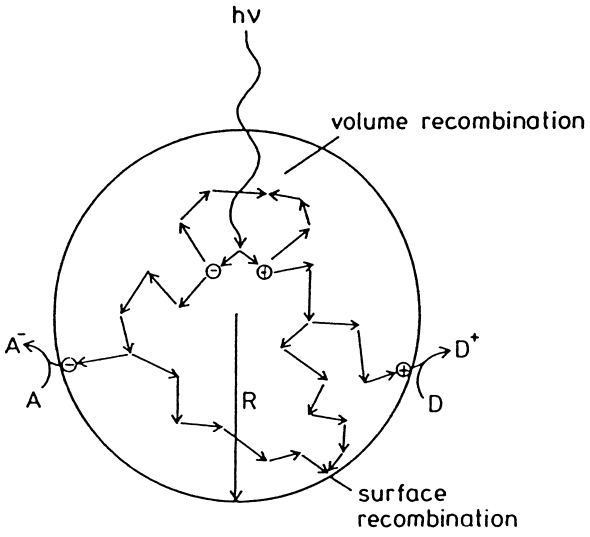

Fig. 2. Fate of electrons and holes within a spherical particle of titania in the presence of acceptor (A) and (D) molecules (after late Dr.H. Gerisher, p. 1 in ref. [3]).

generally observed, the best photocatalytic performances with maximum quantum yields are always obtained with titania. In addition, anatase is the most active allotropic form among the various ones available, either natural (rutile and brookite) or artificial (TiO_2–B, TiO_2–H). Anatase is thermodynamically less stable than rutile, but its formation is kinetically favored at lower temperature (<600°C). This lower temperature could explain higher surface area, and a higher surface density of active sites for adsorption and for catalysis. In all the systems described in the present paper, the catalyst used was titania (Degussa TiO_2 P-25, 50 m^2/g, mainly anatase), unless otherwise stated.

Depending on the reaction considered, various photoreactors can be chosen:

- fixed-bed photoreactors,
- slurry batch photoreactors either mechanically or magnetically stirred.

In laboratory experiments, near-UV light was provided by a Philips lamp (HPK 125 W) placed in front of an the optical window of the photoreactor. IR beams were removed by a circulating-water cell. The wavelength was adjusted with optical filters (fused silica, or pyrex, or Corning glass filters). The radiant flux was measured with a radiometer (Radiometer Technology Model 21A) calibrated against a calorimeter.

For solar detoxification, the experimental pilot photoreactor of PSA was used, which has been thoroughly described by Malato et al. [8]

3. Influence of physical parameters governing the kinetics

3.1. Mass of Catalyst

Either in static, or in slurry or in dynamic flow photoreactors, the initial rates of reaction were found to be directly proportional to the mass *m* of catalyst (Fig. 3(A)). This indicates a true heterogeneous catalytic regime. However, above a certain value of *m*, the reaction rate levels off and becomes independent of *m*. This limit depends on the geometry and on the working conditions of the photoreactor. It was found equal to 1.3 mg TiO_2/cm^2 of a fixed bed and to 2.5 mg TiO_2/cm^3 of suspension. These limits correspond to the maximum amount of TiO_2 in which all the particles – i.e., all the surface exposed – are totally illuminated. For higher quantities of catalyst, a screening effect of excess particles occurs, which masks part of the photosensitive surface. For applications, this optimum mass of catalyst has to be chosen in order to avoid excess of catalyst and (ii) to ensure a total absorption of efficient photons. In laboratory experiments, using a batch photoreactor, an optimum of TiO_2 concentration of 2.5 g/l was found, whereas for the CPC solar reactor at PSA, which is a recirculation plug flow reactor corresponding to a batch reactor, the optimum titania concentration was only 0.2 g/l.

3.2. Wavelength

The variations of the reaction rate as a function of the wavelength follows the absorption spectrum of the catalyst (Fig. 3(B)), with a threshold corresponding to its band gap energy. For TiO_2 having $E_G = 3.02$ eV, this requires: $\lambda \leq 400$ nm, i.e., near-UV wavelength (UV-A). In addition, it must be checked that the reactants do not absorb the light to conserve the exclusive photoactivation of the catalyst for a true heterogeneous catalytic regime (no homogeneous nor photochemistry in the adsorbed phase).

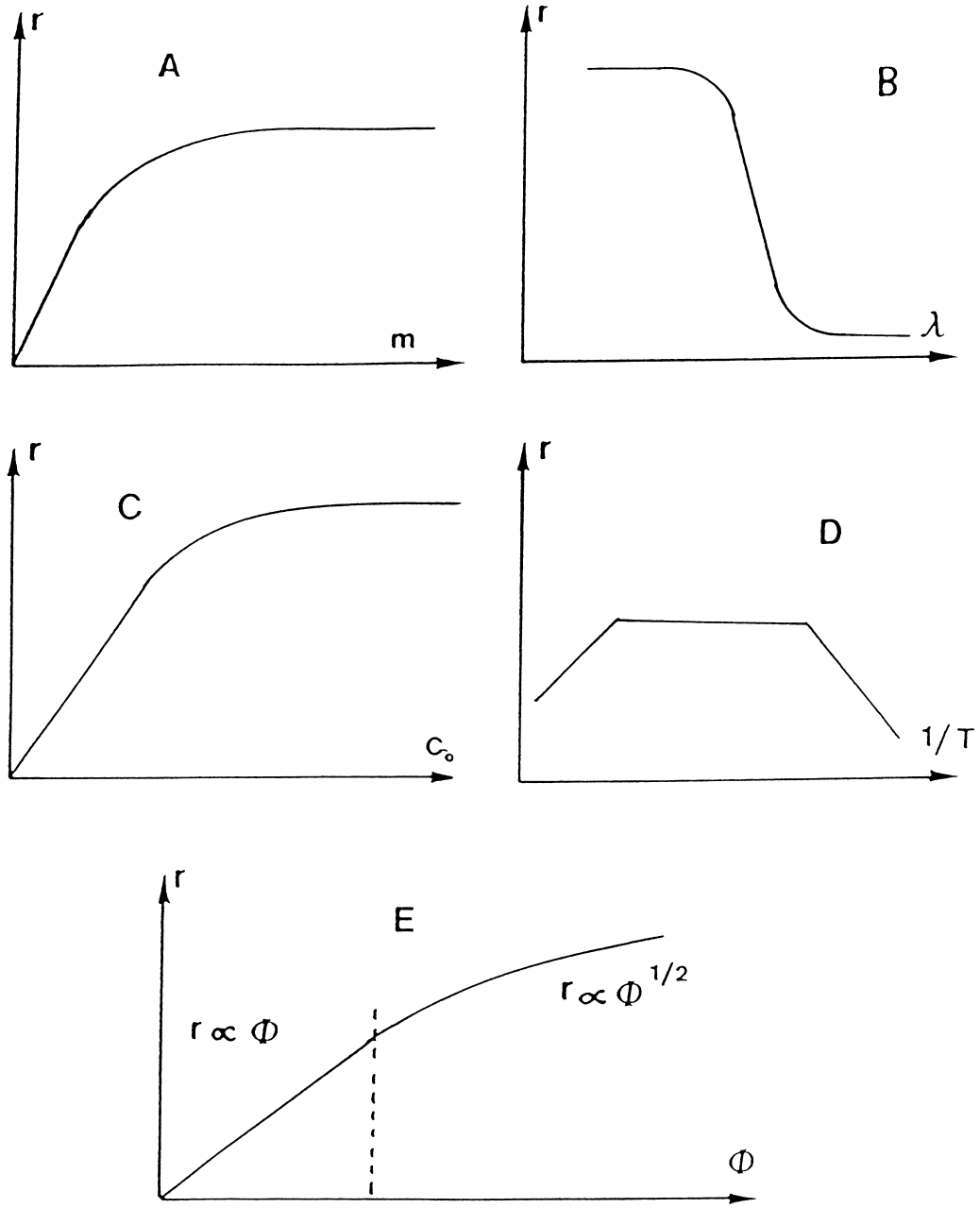

Fig. 3. Influence of the different physical parameters which govern the reaction rate r (r is generally comprised between 1 and 0.1 mmol/h): (A) mass of catalyst; (B) wavelength; (C) initial concentration of reactant; (D) temperature; (E) radiant flux.

3.3. Initial concentration

Generally, the kinetics follows a Langmuir–Hinshelwood mechanism confirming the heterogeneous catalytic character of the system with the rate r varying proportionally with the coverage θ as:

$$r = k\theta = k\left(\frac{KC}{1+KC}\right). \tag{5}$$

For diluted solutions ($C < 10^{-3}$ M), KC becomes $\ll 1$ and the reaction is of the apparent first order, whereas for concentrations $>5 \times 10^{-3}$ M, ($KC \gg 1$), the reaction rate is maximum and of the zero order (Fig. 3(C)).

3.4. Temperature

Because of the photonic activation, the photocatalytic systems do not require heating and are operating at room temperature. The true activation energy E_t is nil, whereas the apparent activation energy E_a is often very small (a few kJ/mol) in the medium temperature range ($20^\circ C \leq \theta \leq 80^\circ C$). However, at very low temperatures ($-40^\circ C \leq \theta^\circ C \leq 0^\circ C$), the activity decreases and the apparent activation energy E_a increases (Fig. 3(D)). The rate limiting step becomes the desorption of the final product and E_a tends to the heat of adsorption of the product. This has been checked for reactions involving hydrogen (alcohol dehydrogenation [9,10] or alcane-deuterium isotopic exchange [11]), carried out on bifunctional Pt/TiO_2 photocatalysts. The E_a was found equal to +10 kcal/mol (+42 kJ/mol), which just corresponds to the heat Q_{H_2} (ads) (or to the opposite of the enthalpy ΔH_{H_2} (ads)) of the reversible adsorption of H_2 on platinum measured by microcalorimetry [12].

On the opposite, when $\theta^\circ C$ increases above $80^\circ C$ and tends to the boiling point of water, the exothermic adsorption of reactant A becomes disfavored and tends to become the rate limiting-step. Correspondingly, the activity decreases and the apparent activation energy becomes negative tending to Q_A (Fig. 3(D)).

As a consequence, the optimum temperature is generally comprised between 20 and $80^\circ C$. This explains why solar devices which use light concentrators require coolers [13]. This absence of heating is attractive for photocatalytic reactions carried out in aqueous media and in particular for environmental purposes (photocatalytic water purification). There is no need to waste energy in heating water which possesses a high heat capacity. This explains why photocatalysis is cheaper than incineration [14].

3.5. Radiant flux

The rate of reaction r is proportional to the radiant flux Φ (Fig. 3(E)). This confirms the photo-induced nature of the activation of the catalytic process, with the participation of photo-induced electrical charges (electrons and holes) to the reaction mechanism. However, above a certain value, estimated to be ca. 25 mW/cm^2 in laboratory experiments, the reaction rate r becomes proportional to $\Phi^{1/2}$. The optimal light power utilization corresponds to the domain where r is proportional to Φ.

3.6. Quantum yield

By definition, it is equal to the ratio of the reaction rate in molecules per second (or in mols per second) to the efficient photonic flux in photons per second (or in Einstein per second (an Einstein is a mol of photons)). This is a kinetic definition, which is directly related to the instantaneous efficiency of a photocatalytic system. Its theoretical maximum value is equal to 1. It may vary on a wide range according (i) to the nature of the catalyst; (ii) to the experimental conditions used (concentrations, T, m, ...) and (iii) especially to the nature of the reaction considered. We have found values comprised between 10^{-2} and 70%. The knowledge of this parameter is fundamental. It enables one (i) to compare the activity of different catalysts for the same reaction, (ii) to estimate the relative feasibility of different reactions, and (iii) to calculate the energetic yield of the process and the corresponding cost.

3.7. Influence of oxygen pressure

For liquid phase reactions, it was difficult to study the influence of P_{O_2} because the reaction is polyphasic. It is generally assumed that oxygen adsorbs on titania from the liquid phase, where it is dissolved following Henry's law. If the oxygen is regularly supplied, it can be assumed that its coverage at the surface of titania is constant and can be integrated into the apparent rate constant:

$$A + O_2 \rightarrow P$$

$$r_A = \frac{-d[A]}{dt} = k\theta_A\,\theta_{O_2} = k_{app}\,\theta_A$$

Actually, the apparent rate constant is a function of the power flux (expressed in mW/cm^2) and of the oxygen coverage.

4. Photocatalytic mild oxidations versus total oxidations

The gas phase or the pure liquid organic phase oxidations using oxygen from the air as the oxidizing agent mainly concerned the mild oxidation of alkanes, alkenes, alcohols and aromatics into carbonyl-containing molecules [15–18]. For instance, cyclohexane and decaline were oxidized into cyclohexanone and 2-decalone, respectively, with an identical selectivity of 86% [17]. Aromatic hydrocarbons [18] such as alkyltoluenes or *o*-xylenes were selectively oxidized on the methylgroup into alkylbenzaldehyde:

$$CH_3–C_6H_4–R + O_2 \rightarrow CHO–C_6H_4–R + H_2O \quad (6)$$

Pure liquid alcohols were also oxidized into their corresponding aldehydes or ketones. In particular, the oxidation of isopropanol into acetone was chosen as a photocatalytic test for measuring the efficiency of passivation of TiO_2 or ZnO based pigments in painting against weathering. The high selectivity was ascribed to a photoactive neutral, atomic oxygen species [15–18]

$$O^-(ads) + p^+ \rightarrow O^* \quad (7)$$

By contrast, as soon as water is present, the selectivity turns in favor of total oxidative degradation. This was ascribed to the photogeneration of stronger, unselective, oxidant species, namely $OH^\bullet$ radicals originating from water via the OH^- groups of titania's surface:

$$(H_2O \leftrightarrow H^+ + OH^-) + p^+ \rightarrow H^+ + OH^\bullet$$
$$\overset{\text{substrate}}{\rightarrow} \text{Intermediates} \rightarrow \text{Final Products}$$
$$(CO_2, H_2O, X^-, A^- \ldots) \quad (8)$$

This system is the most promising issue for an application of heterogeneous photocatalysis, since it is directly connected to water detoxification and to pollutant removal in aqueous effluents. It will be described in the next section.

5. Photocatalytic water decontamination by total mineralization of organic pollutants

5.1. Disappearance of the pollutant

Most of the pollutants which are in the non-exhaustive list, given in Table 1, disappear following an apparent first order kinetics (see Section 3.3). For aromatics, the dearomatization is rapid even in the case of deactivating substituents on the aromatic ring. This was observed for the following substituents: Cl [19,20], NO_2 [21], $CONH_2$ [22], CO_2H [19] and OCH_3 [23]. If an aliphatic chain is bound to the aromatic ring, the breaking of the bond is easy as was observed in the photocatalytic decomposition of 2,4-D (2,4-dichlorophenoxyacetic acid) [24,25] and tetrachlorvinphos ((Z)-2-chloro-1 (2,4,5-trichlorophenyl) ethenyl dimethyl phosphate) [26], and phenitrothion [27].

5.2. Total mineralization

The oxidation of carbon atoms into CO_2 is relatively easy. It is, however, in general markedly slower than the dearomatization of the molecule. Until now, the absence of total mineralization has been observed only in the case of s-triazines herbicides, for which the final product obtained was essentially 1,3,5-triazine-2,4,6, trihydroxy (cyanuric acid) [28], which is, fortunately, not toxic. This is due to the high stability of the triazine nucleus, which resists most oxidation methods. For chlorinated molecules, Cl^- ions are easily released in the solution [19,20] and this could be of interest in a process, where photocatalysis would be associated with a biological depuration system which is generally not efficient for chlorinated compounds. Nitrogen-containing molecules are mineralized into NH_4^+ and mostly NO_3^- [22]. Ammonium ions are relatively stable and the proportion depends mainly on the initial oxidation degree of nitrogen and on the irradiation time [29]. The pollutants containing sulfur atoms are mineralized into sulfate ions [26,27,29]. Organophosphorous pesticides produce phosphate ions [26,27,30,31]. However, phosphate ions in the pH range used remained adsorbed on TiO_2. This strong adsorption partially inhibits the reaction rate which, however, remains acceptable

Table 1
Non-exhaustive list of aqueous organic pollutants mineralized by photocatalysis[a]

Class of organics	Examples
Alkanes	isobutane, pentane, heptane, cyclohexane, paraffins
Haloalkanes	mono-, di-, tri- and tetrachloromethane, tribromoethane, 1,1,1-trifluoro-2,2,2 trichloroethane
Aliphatic alcohols	methanol, ethanol, propanol, glucose
Aliphatic carboxylic acids	formic, ethanoic, propanoic, oxalic, butyric, malic acids
Alkenes	propene, cyclohexene
Haloalkenes	1,2-dichloroethylene, 1,1,2-trichloroethylene
Aromatics	Benzene, naphthalene
Haloaromatics	chlorobenzene, 1,2-dichlorobenzene
Nitrohaloaromatics	dichloronitrobenzene
Phenolic compounds	phenol, hydroquinone, catechol, methylcatechol, resorcinol, *o*- *m*-, *p*-cresol, nitrophenols
Halophenols	2-, 3-, 4-chlorophenol, pentachlorophenol, 4-fluorophenol,
Amides	Benzamide
Aromatic carboxylic acids	benzoic, 4-aminobenzoic, phthalic, salicylic, *m*- and *p*-hydroxybenzoic, chlorohydroxybenzoic and chlorobenzoic acids
Surfactants	sodium dodecylsulphate, polyethylene glycol, sodium dodecyl benzene sulphonate, trimethyl phosphate, tetrabutylammmonium phosphate
Herbicides	atrazine, prometron, propetryne, bentazon, 2-4 D, monuron
Pesticides	DDT, parathion, lindane, tetrachlorvinphos, phenitrothion...
Dyes	methylene blue, rhodamine B, methyl orange, fluorescein

[a] A rather complete list of all photocatalytically degradable pollutants has been established by D. Blake (ref. [7])

[26,27,32]. Until now, the analyses of aliphatic fragments resulting from the degradation of the aromatic ring have only revealed formate and acetate ions. Other aliphatics (presumably acids, diacids, hydroxylated compounds) are very difficult to separate from water and to analyze. Formate and acetate ions are rather stable, as observed in other advanced oxidation processes, which in part explain why the total mineralization is much longer that the dearomatization reaction.

5.3. Degradation pathways

Primary intermediates detected and identified by HPLC and GC/MS of the photocatalytic degradation of various aromatic pollutants correspond to the hydroxylation of the benzene ring. These intermediates have very low transient maximum concentrations with respect to that of the initial pollutant in agreement with the fact that CO_2, acetate and formate are formed in the initial stages of the degradation. The orientation of the hydroxylation of the aromatic ring depends on the nature of the substituents. For instance, for chlorophenols and dimethoxybenzenes, the *para* and *ortho* positions (with respect to OH for the chlorophenols) are favored as is expected. By contrast, for benzamide and nitrobenzene, the hydroxylation occurs at all free sites, whereas a meta orientation is expected for electron-withdrawing substituents. The degradation pathways are illustrated here by the examples of fenitrothion (Fig. 4) and of malic acid (Fig. 5).

Fenitrothion is a powerful insecticide and has the following formula:

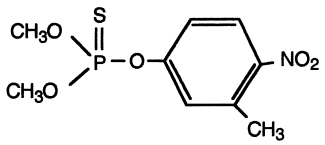

It has been shown, according to the mass balance analysis, that it was photocatalytically degraded according to the overall equation:

$$(CH_3O)_2 - P(S) - O - C_6H_3 - (NO_2)(CH_3) + \frac{13}{2}O_2 \rightarrow 9CO_2 + 3H_2O + 4H^+ + H_2PO_4 + SO_4{}^{2-} + NO_{3-} \quad (9)$$

Malic acid is present in biomass (fermentation processes) and has been chosen as a model molecule for carboxylic acids, which are the main constituents of intermediate products in oxidative degradation processes. In Fig. 5, the main pathway is the second one

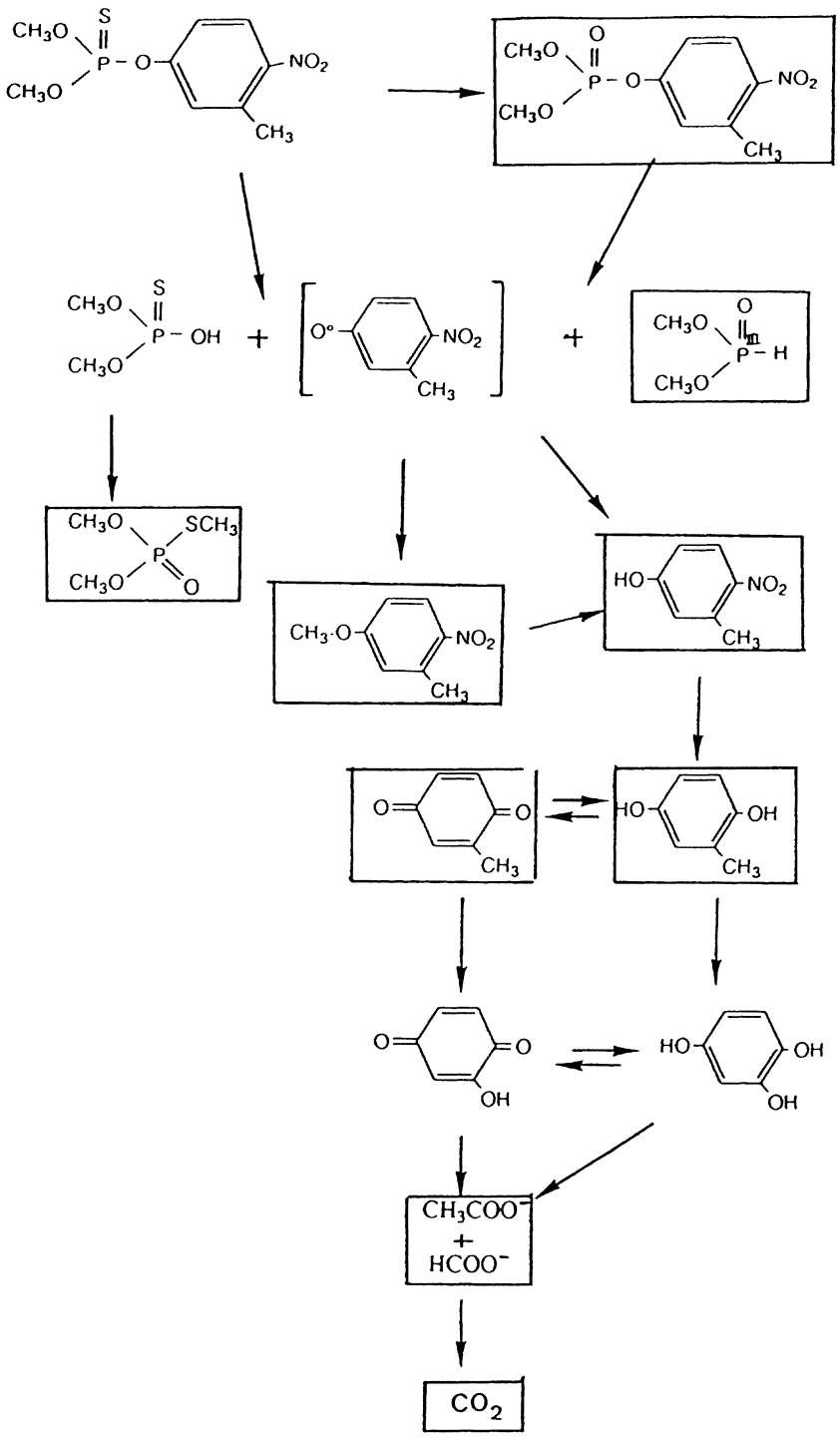

Fig. 4. Schematic photocatalytic degradation pathway of fenitrothion. (The enclosed molecules correspond to those detected).

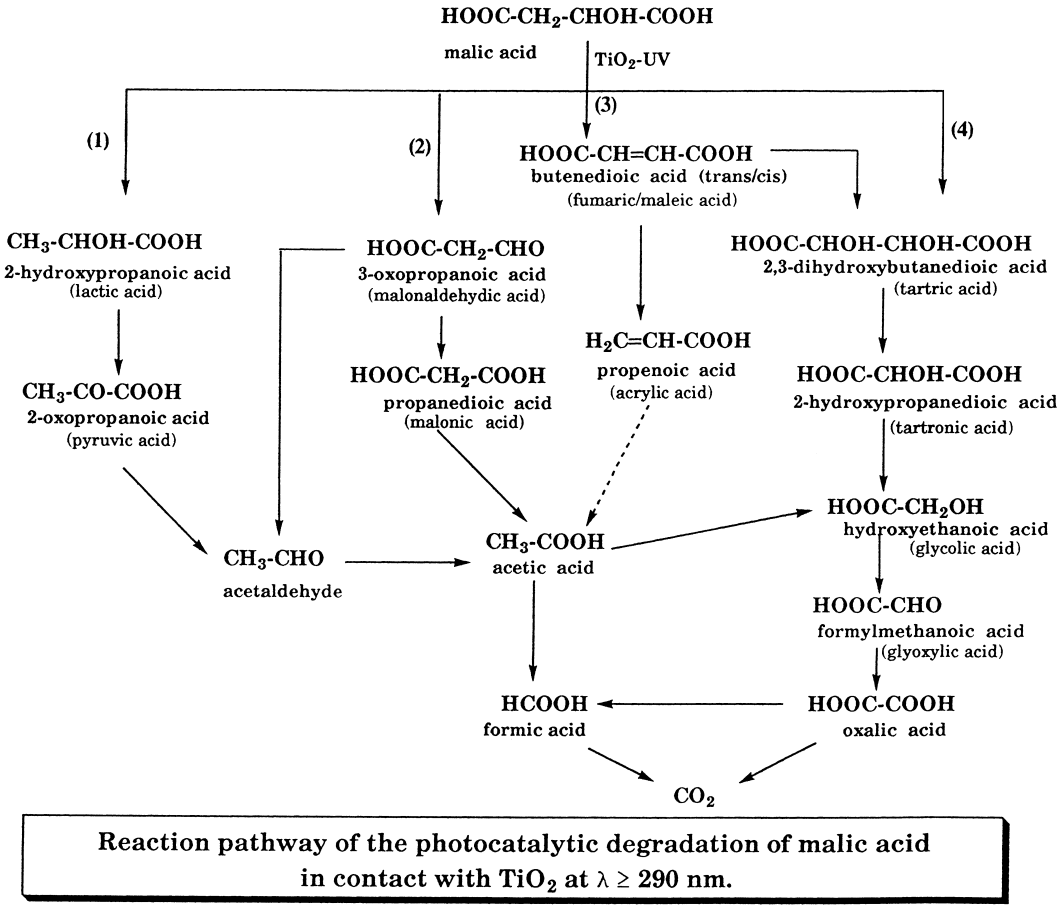

Fig. 5. Schematic photocatalytic degradation pathway of malic acid.

with the formation of malonaldehydic acid. The first decarboxylation, according to a 'photo-Kolbe' reaction:

$$R - COO^- + p^+ \rightarrow R^\bullet + CO_2 \quad (10)$$

seems to concern to carboxylic group in α of the OH group, in line with a higher affinity of this extremity of the molecule for chemisorption on the hydroxylated surface of titania. It can be noted that in Path 3, the formation of maleic-fumaric acids corresponds to a photo-assisted dehydration which constitutes a rare example of a photocatalytic reaction which does not imply a variation of the oxidation degree of carbon.

5.4. Photocatalytic treatment of a real highly loaded industrial waste water

Whereas academic studies have to be done in single-constituent model solutions, real waste waters contain a lot of compounds, both organic and inorganic. The possible interferences between two reactants have been followed during the simultaneous photodegradation of phenol and of (i) methanol, (ii) acetone, (iii) formamide and (iv) acetate ions, respectively [33]. Only acetate ions gave condensation products with phenol (phenylacetate, toluene and acetophenone), resulting from radicals generated by the photo-Kolbe reaction ($CH_3^\bullet$, $CH_3COO^\bullet$) of acetate. This indicated that some condensation products can be formed between reactants but for-

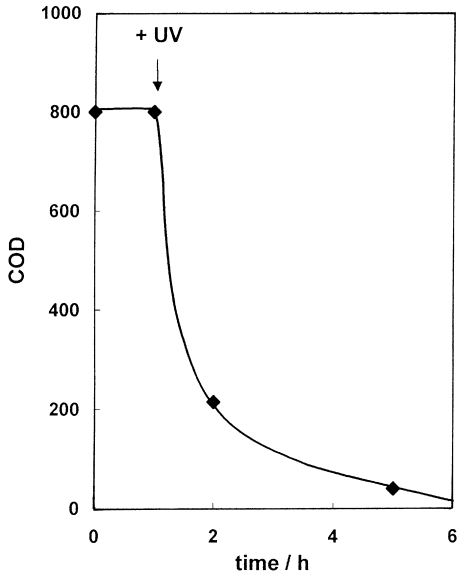

Fig. 6. Kinetics of decrease of the chemical oxygen demand (COD in mg/kg) during the photocatalytic treatment of the real industrial waste water described in Table 2 (diluted 1000 times).

tunately they are promptly mineralized by photocatalysis.

A highly loaded real industrial waste water was treated using photocatalysis. Its characteristics are listed in Table 2. This fetid bad-smelling black solution was initially (i) too highly loaded with respect to the photonic flux used and (ii) too dark for an easy irradiation of the catalyst. It was diluted 1000 times and treated for 4 h. The decrease in the overall pollutant content was monitored by measuring the chemical oxygen demand (COD) (Fig. 6). After an adsorption period (1 h) in the dark, COD decreased by 95% in 4 h. This demonstrated that photocatalysis could be very efficient in a reasonable time for treating black waste waters, which turned clear and lost their bad smell, in agreement with the detoxification and decolorizing of used waters from olive oil industry [34].

6. Inorganic pollutant detoxification or removal

6.1. Inorganic anions

Various toxic anions can be oxidized into harmless or less toxic compounds by using TiO_2 as a photocatalyst. For instance, nitrite is oxidized into nitrate [35,36], sulfide, sulfite [37] and thiosulfate [38] are converted into sulfate, whereas cyanide is converted either into isocyanide [39] or nitrogen [40] or nitrate [41].

6.2. Noble metal recovery

Heavy metals are generally toxic and can be removed from industrial waste effluents [38,42] as small crystallites deposited on the photocatalyst according to the redox process:

$$M^{n+} + H_2O \underset{\text{semiconductor}}{\overset{h\nu}{\rightarrow}} M^{\circ} + nH^{+} + \frac{n}{4}O_2 \qquad (10)$$

provided the redox potential of the cation metal couple is higher than the flat band potential of the semiconductor.

Under identical conditions, the following reactivity pattern was found:

$$Ag > Pd > Au > Pt \gg Rh \gg Ir \gg Cu = Ni = Fe = 0 \qquad (11)$$

For silver, the deposition initially occurred by forming small crystallites between 3 and 8 nm [38]. As the photodeposition conversion increased, the metal particles form agglomerates, reaching several hundreds of nm (i.e., bigger than the TiO_2 particles) [38]. Since these agglomerates contained a major part of the metal deposited, the photosensitive surface was not markedly masked and relatively high amounts of metals were recovered. The final concentration is lower than the detection limits of atomic absorption spectroscopy ($\leq$0.01 ppm). Silver photodeposition has been applied with two environmental interests: (i) the recovery of Ag from used photographic baths in which the silver-thiosulfate complex is decomposed, Ag^+ being reduced to Ag° and (ii) the detoxification of the aqueous effluent, $S_2O_3{}^{2-}$ being oxidized into innocuous $SO_4{}^{2-}$, whereas phenolic compounds are degraded into CO_2 [43].

From an application point of view, the recovery of silver from photographic baths seems to be the most promising issue, provided the legislation towards Ag-containing discharge waters becomes more strict. It can also be noted that photodeposition is working with the recovery of Hg^{2+}.

Table 2
Composition and characteristics of a highly loaded industrial waste water treated by photocatalysis

Organic compounds		wt.% min	wt.% max
1-sulfocyclohexane-1-carboxylic acid		8	12.5
ϵ-amino-caproic acid		0.3	4.0
N-cyclohexyl-e-aminocaproic acid:	C_6H_{11}–CO–NH–$(CH_2)_5$–COOH		1.8
Cyclohexyl-formic acid	C_6H_{11}–COOH	0.1	
		0.2	2
Caprolactam	$(CH_2)_5$–CO–NH	0.02	1.6
Benzoic acid	C_6H_5–COOH	0.01	0.5
N-cyclohexy1-5 amino-valeric acid:	C_6H_5–CO–NH–$(CH_2)_4$–COOH	0.01	0.3
Adipic acid	COOH–$(CH_2)_2$–COOH	0.01	0.25
Methyl-cyclohexenyl-formic acid	CH_3–C_6H_8–COOH	0.03	0.25
Cyclohexenyl-formic acid	C_6H_9–COOH	0.02	0.25
γ-caprolactone		0.01	0.25
Methyl-valero-lactone		0.01	0.25
Other organic compounds		ppm min	ppm max
Phenol		60	150
2-chlorophenol		1	20
2,4-dichorophenol		0.01	2
		0.01	1
2,4,6-trichorophenol		0.05	10
Toluene		0.01	0.5
Benzene, hexane			
Inorganic compounds		ppm min	ppm max
Nitrites		50	100
Nitrates		150	350
Iron		10	80
Chromium		0.5	4
Co, Mn, Al, Cu, Zn		0.2	5
		–	59 g/l
Sodium			1
Potassium			30
Calcium			78%
Water		66%	
Characteristics of the solution			
Density		1.1 kg/l	1.2 kg/l
pH		10	10
Solid residue % after drying at 105°		22%	34%
Total Organic Carbon (TOC)			113 000
Chemical Oxygen Demand (COD)			800 000

7. Polyphasic (solar) photoreactors

To perform the various types of photocatalytic reactions described above, different types of photoreactors have been built with the catalyst used under various shapes: fixed bed, magnetically or mechanically agitated slurries, catalyst particles anchored on the walls of the photoreactor or in membranes or on glass beads, or on glass-wool sleeves, small spherical pellets, etc. [1–4]. The main purpose is to have an easy separation of the catalyst from the fluid medium, thence the necessity to support titania and to avoid ultrafine particles filtration.

Various devices have been developed such as TiO_2-coated tubular photoreactors, annular and spiral photoreactors, falling-film photoreactors. At present

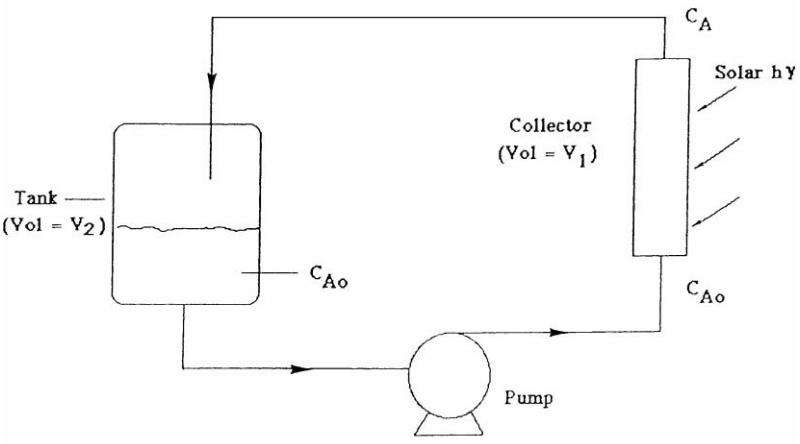

Scheme of the CPC photoreactor at PSA

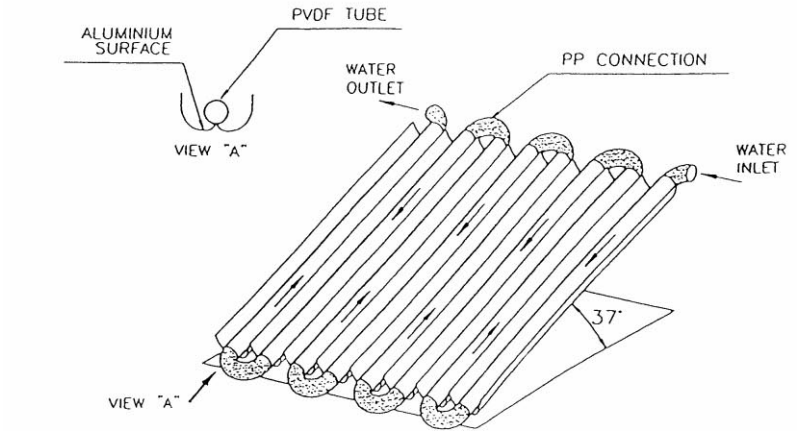

Fig. 7. Scheme and description of the CPC solar photoreactor at PSA (Spain).

two systems are commercialized [44,45]. One uses powder TiO_2 and concerns the market of waste water treatment. In the other system, TiO_2 is supported on a fiber glass mesh cloth in which a cylindrical UV lamp is wrapped. Very recently an evaluation of ultraviolet oxidation methods was carried out for the removal of 2, 4, 6-trinitrotoluene from groundwater [6,46] These methods were powder TiO_2/UV, O_3/UV, H_2O_2 + additive/UV. Heterogeneous photocatalysis was found to be the most economical. Even though several criticisms can be made to this evaluation, it comes out that heterogeneous photocatalysis appears as a method that can compete economically with other UV oxidation processes for water treatment.

The most effective photocatalysts are anatase samples which absorb only ca. 3% of the overall solar energy at the earth's surface. In spite of that, large-scale tests have been built or modified and are still used in North America, Israel and Europe [46–48] to collect data in order to estimate the cost of water treatment. Solar reactors that do not concentrate the incident light have lower hardware cost, eliminate photon losses at reflecting surfaces and use diffused sunlight [47–49]. For these non-concentrating systems, estimates have concluded that solar photons can be used at a lower cost than photons from UV lamps [46].

7.1. Photocatalytic degradation of aqueous pollutants in a solar pilot plant

The principle of the CPC photoreactor at PSA (Plataforma Solar de Almeria, Spain) is described in the schemes of Fig. 7. The collector has an inclination angle of 37° corresponding to the latitude of Almeria. The CPC collector which is the irradiated part of the system corresponds to a plug flow reactor but, since it is connected to a tank and a recirculation pump, the ensemble corresponds to a batch reactor. The solar photocatalytic degradation of pollutants in the CPC photoreactor has been successfully applied at PSA on various pollutants [8,49–51]. These experiments can be exemplified by the total mineralization of benzofuran (BZF), a representative of aromatic polycyclic hydrophobic contaminants [51].

After an adsorption period of 1 h in the dark, BZF disappeared following a first order kinetics (Fig. 8), as confirmed by the linear transform of Fig. 9. The

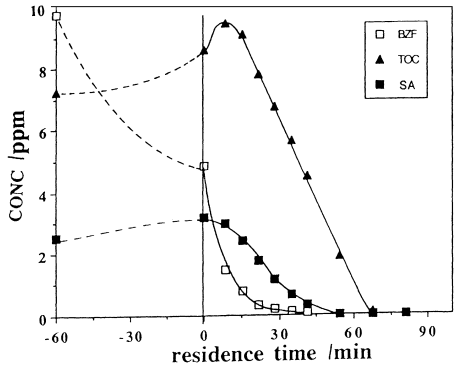

Fig. 8. Kinetics of (i) BZF and TOC disappearance, and (ii) of salicylic aldehyde (SA) appearance and disappearance.

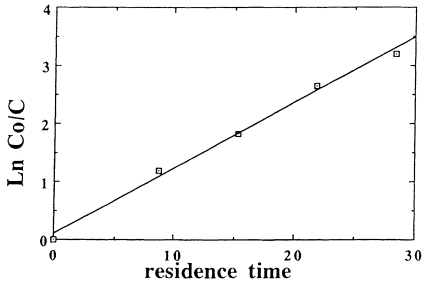

Fig. 9. First order linear transform ln $(C_0/C) = f(t_R)$ of the kinetics of BZF disappearance.

TOC decreased linearly to 0 within 1 h with an apparent zeroth kinetic order, that could be interpreted by assuming a saturation of surface sites by all the intermediates

$$\frac{-\mathrm{d[TOC]}}{\mathrm{d}t} = \frac{+\mathrm{d[CO_2]}}{\mathrm{d}t} = k\sum\theta_i = k\sum\frac{K_iC_i}{1+K_iC_i} \sim k\,\theta_{\mathrm{sat}} \sim k \qquad (12)$$

where θ_i represents the surface coverage int the *i*th intermediate and θ_{sat} the overall coverage at saturation. The first order linear transforms ln $C_o/C = f(t)$ for BZF at different dates with different UV-radiant fluxes indicated that the rate constant of BZF disappearance is quite proportional to the mean UV power flux. This means, according to Fig. 3(E), that the CPC is working in optimal conditions with respect to solar irradiation and can also work with diffuse UV-light.

These experiments were compared with initial studies performed in a laboratory microphotoreactor working with artificial light. Despite a volume extrapolation

factor of 12 500, the same first order was found for BZF disappearance; the intermediates were the same, indicating an identical reaction pathway; the quantum yields were the same. Only two points of apparent divergence were observed: (i) the optimum concentration in titania for the CPC pilot plant was 0.2 g/l instead of 2.5 g/l for the batch microreactor; and (ii) the TOC disappearance at PSA was faster than the CO_2 evolution in laboratory experiments. This was ascribed to the CPC photoreactor design [8,51] with a recirculating tank which favors the production of the final products detrimentally to that of the intermediate ones [52].

The photocatalytic degradation at PSA is being to be applied to the treatment of waste waters contaminated by a large variety of pesticides after the washing of shredded empty herbicide containers (about 1.5 million collected per year), in a plant built for the decontamination and the recycling of plastic. Indeed, herbicides are intensively used in the province of Almeria, which has become an important producer of fruit and vegetables in green houses because of the very sunny climate. If the demonstration of the technical and economical feasibility of the process is achieved, the city of El Ejido, located in the center of the green house area, will become the first European town to include a solar photocatalytic plant in a real waste treatment process.

This could also be the first project in heterogeneous photocatalysis to make the jump from the laboratory to the industrial scale.

8. Conclusions

Water pollutant removal appears as the most promising potential application since many toxic water pollutants, either organic or inorganic, are totally mineralized or oxidized at their higher degree, respectively, into harmless final compounds. Besides some drawbacks (use of UV-photons and necessity for the treated waters to be transparent in this spectral region; slow complete mineralization in cases where heteroatoms are at a very low oxidation degree; photocatalytic engineering to be developed), room-temperature heterogeneous photocatalysis offers interesting advantages [5]:

- chemical stability of TiO_2 in aqueous media and in large range of pH ($0 \leq pH \leq 14$)
- low cost of titania (~10 FF/kg or 1.54 EURO/kg)
- cheap chemicals in use.
- no additives required (only oxygen from the air).
- system applicable at low concentrations.
- great deposition capacity for noble metal recovery.
- absence of inhibition or low inhibition by ions generally present in water.
- total mineralization achieved for many organic pollutants.
- efficiency of photocatalysis with halogenated compounds sometimes very toxic for bacteria in biological water treatment.
- possible combination with other decontamination methods (in particular biological).

Heterogeneous photocatalysis is now reaching the preindustrial level. Several pilots and prototypes have been built in various countries [3]. The solar photocatalytic treatment of pesticides used in agriculture and in food industry, which is under study at PSA for Almeria province, is an excellent example of the emerging development of solar water detoxification.

Appendix List of symbols

Symbols	Significance	Units
e^-	electron	$-(1.602\ 06 \pm 0.000\ 03 \times 10^{-19}$C
p^+	hole or position	$+ (1.602\ 06 \pm 0.000\ 03) \times 10^{-19}$C
h	Planck's constant	$6.625\ 17 \pm 0.00023 \times 10^{-34}$ J s
ν	frequency of the UV radiation	Hz
N	neutral center	dimensionless
θ	surface coverage	dimensionless
r	reaction rate	mol/s
k	rate constant	1st order: s^{-1} 0th order: mol/s
Φ	radiant flux	mW cm^{-2}
ΔH_{ads}	enthalpy of adsorption	kJ/mol
Q_{ads}	heat of adsorption counted positive ($Q = -\Delta H$)	kJ/mol
TOC	total organic carbon	mg C/l

References

[1] M. Schiavello (Ed.), Photocatalysis and Environment, Kluwer Academic Publishers, Dordrecht, 1988.
[2] N. Serpone, E. Pelizzetti (Eds.), Photocatalysis, Fundamentals and Applications, Wiley, New York, 1989.
[3] D.F. Ollis, H. Al-Ekabi (Eds.), Photocatalytic Purification, and Treatment of Water and Air, Elsevier, Amsterdam, 1993.
[4] O. Legrini, E. Oliveros, A. Braun, Chem. Rev. 93 (1993) 671.
[5] J.M. Herrmann, C. Guillard, P. Pichat, Catal. Today 17 (1993) 7.
[6] D.W. Bahnemann, J. Cunningham, M.A. Fox, E. Pelizzetti, P. Pichat, N. Serpone, in: Aquatic Surface Photochemistry, R.G. Zepp, G.R. Helz, D.G. Crosby (Eds.), F.L. Lewis Publishers, Boca Raton, 1994, p. 261.
[7] D.M. Blake, Bibliography of Work on Photocatalytic Removal of Hazardous Compounds from Water and Air, NREL/TP-430-22197, National Renewable Energy Laboratory, Golden, 1997.
[8] S.Malato, Ph.D. Dissertation, Almeria University, Spain, 1997
[9] P. Pichat, J.M. Herrmann, J. Disdier, H. Courbon, M.N. Mozzanega, Nouv. J. Chim. 5 (1981) 27.
[10] P. Pichat, J.M. Herrmann, J. Disdier, H. Courbon, M.N. Mozzanega, Nouv. J. Chim. 6 (1982) 53.
[11] H. Courbon, J.M. Herrmann, P. Pichat, J. Catal. 95 (1985) 539.
[12] J.M. Herrmann, M. Gravelle-Rumeau-Mailleau, P.C. Gravelle, J. Catal. 104 (1987) 136.
[13] C. Turchi, M. Mehos, J. Pacheco in ref. [3], p. 789.
[14] R. Miller, R. Fox in ref [3], p. 573.
[15] J.M. Herrmann, J. Disdier, M.N. Mozzanega, P. Pichat, J. Catal. 60 (1979) 369.
[16] J.M. Herrmann, H. Courbon, J. Disdier, M.N. Mozzanega, P. Pichat, Stud. Surf. Sci. Catal., Elsevier Amsterdam 59 (1990) 675.
[17] J.M. Herrmann, W. Mu, P. Pichat, Stud. Surf. Sci. Catal., Elsevier Amsterdam 55 (1990) 405.
[18] P. Pichat, J. Disdier, J.M. Herrmann, P. Vaudano, Nouv. J. Chim. 10 (1986) 545.
[19] H. Tahiri, Y. Aitichou, J.M. Herrmann, J. Photochem. Photobiol. A: general 114 (1998) 219.
[20] J.C. D'Oliveira, G. Al-Sayyed, P. Pichat, Environ. Sci. Technol. 24 (1990) 990.
[21] C. Maillard-Dupuy, C. Guillard, P. Pichat, New J. Chem. 18 (1994) 941.
[22] C. Maillard, C. Guillard, P. Pichat, New J. Chem. 16 (1992) 821.
[23] L. Amalric, C. Guillard, N. Serpone, P. Pichat, J. Environ. Sci. Health A28 (1993) 1393.
[24] P. Pichat, J.C. D'Oliveira, J.F. Maffre, D. Mas p. 683 in ref [3] (1993)
[25] J.M. Herrmann, J. Disdier, P. Pichat, S. Malato, J. Blanco Appl. Catal. B: Environmental 17 (1998) 15.
[26] M. Kerzhentsev, C. Guillard, J.M. Herrmann, P. Pichat p. 601 in ref [3], 1993.
[27] M. Kerzhentsev, C. Guillard, J.P. Pichat, J.-M. Herrmann, Catal. Today 27 (1996) 215.
[28] E. Pelizzetti, V. Maurino, C. Minero, O. Zerbinati, E. Borgarello, Chemosphere 18 (1989) 1437.
[29] G.K.C. Low, S.R. Mc Evoy, R.W. Matthews, Environ. Sci. Technol. 25 (1991) 460.
[30] K. Harada, T. Hisanaga, K. Tanaka, New J. Chem. 11 (1987) 598.
[31] K. Harada, T. Hisanaga, K. Tanaka, Wat. Res. 24 (1990) 1415.
[32] M. Abdullah, G.K.C. Low, R.W. Matthews J. Phys. Chem. 94 (1990) 6820.
[33] C. Renzi, C. Guillard, J.M. Herrmann, P. Pichat, G. Baldi, Chemosphere 35 (1997) 819.
[34] P.C. Passarinho, A. Soares Vieira, S. Malato, J. Blanco, Proc. 1st Users Workshop Training and Mobility of Researchers Programme at PSA, CIEMAT edn., 1998, p. 7.
[35] A. Zafra, J. Garcia, A. Milis, X. Domenech, J. Mol. Catal. 70 (1991) 343.
[36] Y. Hori, A. Nakatsu, S. Susuki, Chem. Lett. (1985) 1429.
[37] S.N. Frank, A.J. Bard, J. Phys. Chem. 81 (1977) 1484.
[38] J.-M. Herrmann, J.J. Disdier, P. Pichat, J. Catal. 113 (1988) 72.
[39] S.N. Frank, A.J. Bard, J. Am. Chem. Soc. 99 (1977) 303.
[40] H. Hidaka, T. Nakamura, A. Ishizaha, M. Tsuchiya, J. Zhao, J. Photochem. Photobiol. A: Chem. 66 (1992) 367.
[41] C.H. Pollema, J. Hendrix, E.B. Milosavljevic, L. Solujic, J.H. Nelson, J. Photochem. Photobiol. A: Chem. 66 (1992) 235.
[42] J.-M. Herrmann, J. Disdier, P. Pichat, J. Phys. Chem. 90 (1986) 6028.
[43] H. Tahiri, N. Serpone, R. Le van Mao, J. Photochem. Photobiol. A: Chem. 93 (1996) 199.
[44] Matrix Photocatalytic Inc., London, Ont., Canada.
[45] Purifics Environmental Technologies Inc., London, Ont., Canada.
[46] D.M. Blake in Alternative Fuels and the Environment, F. Sterrett (Ed.), Lewis, Boca Raton, FL, 1994, p. 175 and refs therein
[47] Plataforma Solar de Almeria, PSA, Spain.
[48] D. Bockelmann, D. Weichgrebe, R. Goslich, D. Bahnemann, Sol. Energy Mater. Sol. Cells 38 (1995) 441.
[49] S. Malato, J. Blanco, C. Richter, B. Braun, M.I. Maldonado, Appl. Catal. B: Environmental, 1998 (in press)
[50] C. Minero, E. Pelizzetti, S. Malato, J. Blanco, Solar Energy 56 (1996) 421.
[51] J.-M. Herrmann, J. Disdier, P. Pichat, S. Malato, J. Blanco, Appl. Catal. B: Environmental 17 (1998) 15.
[52] O. Levenspiel., Chemical Reaction Engineering, Wiley, New York, 1972, p.175.